SUPPLEMENTARY FIGURES

Fig. S1 – related to Fig. 1: Ectopic expression of WT1 –*KTS*^{GOF} prevents differentiation into steroidogenic cells. (A) Schematic representation of the strategy used to generate *Rosa26: WT1–KTS* mice. SHA: Short homology arm, LHA: Long homology arm. An equivalent strategy was used to knock in the Wt1+KTS cDNA. **(B)** Southern blot showing a positively targeted (left lane) and a negative (right lane) clone. **(C)** WT1 (blue) SF1 (red) and GATA4 (green) immunofluorescence on adrenal sections from CTR and –*KTS*^{GOF} embryos at E12.5, E13.5 and E14.5. **(D)** Hematoxylin and eosin staining on adrenal section from E14.5 (left panels) and E 18.5 (right panels) CTR and –*KTS*^{GOF} embryos. **(E)** *21 hydroxylase* RNA *in situ* hybridization on sections from CTR and –*KTS*^{GOF} E18.5 old embryos. Note the increased signal intensity in the remaining –*KTS*^{GOF} steroidogenic cells. Please note that the cytoplasmic WT1 staining in control adrenals is background. **a**, adrenal gland; **k**, kidney.

Fig. S2 – related to Fig. 2: Adrenals from –*KTS*^{GOF} animals are fully functional. (A) 3βHSD2 (which stains adrenocortical steroidogenic cells of all the zones) and AKR1b7 (*zona fasciculata*) immunostaining shows disorganization of the cortical architecture in –*KTS*^{GOF} mice. While disorganized, the cortical zonation is maintained. **(B)** 20αHSD immunostaining on adrenals from 5 weeks old littermate female mice showing reduction in X-zone in –*KTS*^{GOF} animals. **(C)** Despite the severe phenotype observed, circulating corticosterone levels in adult –*KTS*^{GOF} mice are unchanged (left panel), whereas a slight increase in ACTH is observed (right panel). **(D)** Quantification of cellular size using the program 'cell profiler' showed slight hypertrophy of steroidogenic cells in –*KTS*^{GOF} animals (CTR: 934.93 ± 66.60 pixels, n=14; –*KTS*^{GOF}*;* 1033.91 ± 62.77 pixels, n=9; ***P*<0.005, using student t test). **(E)** RT-Q-PCR performed on RNA extracted from adult adrenal glands shows no significant differences in expression of *Cyp11B1, Cyp11B2, Cyp21A1, Cyp11A1, Sf1*, and *StaR* between wild type and -*KTS*^{GOF} mice. **(F-G)** Hematoxilin and eosin staining showed normal adult gonads in both XX and XY –*KTS*^{GOF} animals and the presence of spermatozoa in epididymis of males (G). *p450scc* **(H)** and *21-hydroxylase* **(I)** RNA *in situ* hybridization of gonadal sections from E 14.5 (XY) and E15.5 (XX)

embryos. **(J)** RT-Q-PCR performed on RNA extracted from E12.5 gonads showed no significant increase of either WT1+ or –KTS isoforms in $–KTS^{GOF}$ samples.

Fig. S3 – related to Fig. 3: Molecular analysis of $–KTS^{GOF}$ adrenals and putative targets. (A) *Ptch1* and *Shh* RNA *in situ* hybridization on E15.5 (C) CTR, $–KTS^{GOF}$ and $+KTS^{GOF}$ embryos. **(B)** Quantification of *Ptch1* and *Shh* messengers. **E14.5:** *Ptch1*, CTR: 100 ± 69.40 n=5, $–KTS^{GOF}$: 195.00 $–KTS^{GOF}$ 24.80, n=6; *Shh*, CTR: 100 ± 30.60, n=6; $–KTS^{GOF}$: 150.29 ± 29.69, n=6. **Adult:** *Ptch1*, CTR; 100 ± 24.11, n=8; $–KTS^{GOF}$: 253.76 ± 186.99, n=6; *Shh*, CTR: 100 ± 85.08, n=7; $–KTS^{GOF}$: 121.25 ± 119.09, n=6. * $P< 0.05$ using student T test. The data presented are normalized for *Hprt1* expression. **(C, D)** Snapshots from UCSC genome browser showing ChIP sequencing data on chromatin from E18.5 kidneys immunoprecipitated with anti WT1 or CTR (DICER) antibodies. WT1 strongly binds to a position -48.5Kb upstream of the *Tcf21* gene (chr10: 22,588,088-22,588,616) corresponding to an evolutionary conserved region (ECR), which was also identified in WT1 ChIPs on $–KTS^{GOF}$ adrenals. No peaks of WT1 binding were instead detected for the ECRs located at positions -1.5Kb (chr10: 22,541,258-22,541,553) and -2.7Kb (chr10: 22,542,363-22,542,597) **(C)**. Alignment of the *Gli1* gene landscape with kidney ChIP seq data showing a peak in the intronic region (chr10:126,775,799-126,776,198) that was also found enriched in WT1 ChIPs on $–KTS^{GOF}$ adrenals **(D)**. Arrows indicate the regions for which WT1 ChIP PCRs (depicted in fig. 3F) were performed.

Fig. S4 – related to Fig. 4: $WT1^+$ cells generate $SF1^+$ and $SF1^-$ (interstitial) adrenocortical cells during development. (A) SF1(red) and GFP (green) immunostaining on adrenal sections from 3 weeks old *WT1:Cre-GFP/mTmG* mice. The GFP signal reflects cells in which mTmG derived GFP has been permanently switched on. **(B-D)** Sections from *Wt1:Cre-ERT2; mTmG* animals force fed at E 14.5. WT1 (red) GFP (green) immunofluorescence on adrenal sections from E 18.5 *Wt1:Cre-ERT2; mTmG* embryos treated with tamoxifen at E14.5 showing differentiated steroidogenic GFP^+ cells (B), $WT1^+$ GFP^+ cells within the cortex (C) and interstitial cortical GFP^+ cells ($WT1^-$) (D). **(E-F)** GFP (green) LacZ (red) WT1 (blue) immunofluorescence on adrenal sections from E18.5 old *Wt1:Cre-ERT2; mTmG; Gli1:LacZ* embryos treated with tamoxifen at E12.5. At least four different populations of cells can be described by the expression of WT1 and GLI1: $WT1^+$

GLI1$^+$ capsular cells (E, arrows), WT1$^+$ GLI1$^-$ capsular (E, arrowheads), WT1$^-$ GLI1$^+$ capsular (E, asterisk) and WT1$^+$ GLI1$^-$ cortical (F, inset). **(G)** Quantification of the number of GFP$^+$ patches of cells within the adrenal cortex of E18.5 embryos and 3 weeks old *Wt1:Cre-ERT2; mTmG* mice treated with tamoxifen at E14.5. The overall number of GFP$^+$ clusters increases from 4.9 ± 2.42 (2.6 ± 1.84 WT1$^+$, 2.3 ± 2.45 WT1$^-$) (N=10) to 16.33 ± 4.78 (1.25 ± 0.84 WT1$^+$, 14.0 ± 4.55 WT1$^-$) (N=5).

Fig. S5 – related to Fig. 5: Adult WT1$^+$ cortical cells are neither steroidogenic nor endothelial cells. (A-C) Sections of adrenal glands from *Wt1:Cre-ERT2; mTmG* mice treated with tamoxifen at 10 to 12 weeks and sacrificed one month after the last administration. *P450scc* **(A)** and *21 hydroxylase* **(B)** RNA *in situ* hybridization demonstrates that under normal conditions the majority of GFP$^+$ cells are non-steroidogenic. **(C)** Likewise no colocalisation between the vascular marker PECAM1 (red) and GFP (green) was detected. (**D**) Similar results were obtained when GFP activation was performed during development.

Fig. S6 – related to Fig. 6: WT1$^+$ cortical clusters increase rapidly after gonadectomy. (A) WT1 (blue) GATA4 (red) and GFP (green) immunofluorescence on a section of an adrenal glands from *Wt1:Cre-ERT2; mTmG* mice gonadectomized after treatement with tamoxifen at 10 to 12 weeks and collected 10 weeks after gonadectomy. **(B)** Schematic representation of the experiment shown in C and D. **(C-D)** Quantification of the number of GFP$^+$ cell clusters in the adrenal cortex of male (C) and female (DC) *Wt1:Cre-ERT2; mTmG* mice gonadectomized after treatement with tamoxifen at 3 weeks. * $P< 0.05$ using student T test.

Table S1 – related to Fig. 2: Adrenal weight in wildtype and -*KTS*^{GOF} mice.

Primers table

Name	Direction	Sequence	Usage
Rosa26 common	sense	AGGGAGCTGCAGTGGAGTAG	genotyping Rosa26:Wt1-KTS mice
Pgk	antisense	GAAAAGGCGCTCCCCTACCC	genotyping Rosa26:Wt1-KTS mice
Rosa WT	antisense	AGCCTGCCCAGAAGACTCCC	genotyping Rosa26:Wt1-KTS mice
Tcf21 S	sense	AGATCCTGGCCAACGACAAG	Tcf21 in situ probe
Tcf21 AS	antisense	CCAGGCTTGCAGTCATTCATG	Tcf21 in situ probe
Tcf21 left	sense	CATTCACCCAGTCAACCTGA	Tcf21 Q-PCR, probe 49
Tcf21 right	antisense	CCACTTCCTTCAGGTCATTCTC	Tcf21 Q-PCR, probe 49
Gli1 left	sense	CTGACTGTGCCCGAGAGTG	Gli1 Q-PCR, probe 84
Gli1 right	antisense	CGCTGCTGCAAGAGGACT	Gli1 Q-PCR, probe 84
Cyp11A1 left	sense	AAGTATGGCCCCATTTACAGG	Cyp11A1 Q-PCR, probe 104
Cyp11A1 right	antisense	TGGGGTCCACGATGTAAACT	Cyp11A1 Q-PCR, probe 104
Cyp11B1 left	sense	GCCATCCAGGCTAACTACAT	Cyp11B1 Q-PCR, probe 11
Cyp11B1 right	antisense	CATTACCAAGGGGGTTGATG	Cyp11B1 Q-PCR, probe 11
Cyp11B2 left	sense	GCACCAGGTGGAGAGTATGC	Cyp11B2 Q-PCR, probe 1
Cyp11B2 right	antisense	CCATTCTGGCCCATTTAGC	Cyp11B2 Q-PCR, probe 1
Cyp21A1 left	sense	AGGAATTCTCCTTCCTCACTTGT	Cyp21A1 Q-PCR, probe 51
Cyp21A1 right	antisense	TGTACCAACGTGCTGTCCTT	Cyp21A1 Q-PCR, probe 51
Sf1 left	sense	TCCAGTGTCCACCCTTATCC	Sf1 Q-PCR, probe 12
Sf1 right	antisense	CGTCGTACGAATAGTCCATGC	Sf1 Q-PCR, probe 12
Star left	sense	TTGGGCATACTCAACAACCA	Star Q-PCR, probe 11
Star right	antisense	ACTTCGTCCCCGTTCTCC	Star Q-PCR, probe 11
Tcf21 ECR2 S	sense	GGGCAGGAGCTAAGAGTAAC	ChIP
Tcf21 ECR2 AS	antisense	GGAGCCCATAAATCTCCACG	ChIP
Tcf21 ECR4 S	sense	ATACTTCTTTTTTCCCCCCTGC	ChIP
Tcf21 ECR4 AS	antisense	GACCATGTTCAAAGCAATCCTC	ChIP
Tcf21 FAR ECR S	sense	CCCTGGGCTTTAATTCTAAC	ChIP
Tcf21 FAR ECR AS	antisense	TAAGCGTTCCAGGAAGGGGG	ChIP
Gli Intron S	sense	GGGCAGAAGCAGCCGTTCAG	ChIP
Gli Intron AS	antisense	GAATGACTTTAGCTCTCATCC	ChIP
WT1+/-KTS common	sense	CACCAAAGGAGACACACAGGT	Wt1 +/- KTS Q-PCR, probe 47
WT1 +KTS AS	antisense	TTCACTTGTTTTACCTGTAT	Wt1 +/- KTS Q-PCR, probe 47
WT1 -KTS AS	antisense	GGGCTTTTCACCTGTATGAG	Wt1 +/- KTS Q-PCR, probe 47
LUPub Fr	sense	AATGAGTCCATCACGCTGAAAC	LHR in situ probe
LUPub Rev	antisense	TAGGATGACGTGGCGATGAGCG	LHR in situ probe

Antibodies table

Protein	Host	Type	Diluition	Secondary	Producer	Reference
WT1	Mouse	monoclonal	1:50	Biothynilated/Streptavidin-Cy3	Dako	6H-F2
WT1 C19	Rabbit	polyclonal	1:100	Biothynilated/Streptavidin-Cy3	Santa Cruz	sc 192
SF1	Rabbit	polyclonal	1:500-1000	AlexaFluor 488	Morohashi K,	Ref.[2]
GFP	Rabbit	polyclonal	1:500	AlexaFluor 488	AbCam	ab290
GFP	Goat	polyclonal	1:200	Cy5	AbCam	ab5450
GATA4	Goat	polyclonal	1:100	Cy5	Santa Cruz	sc 1237
CYP17	Rabbit	polyclonal	1:500	AlexaFluor 488	Conley A.	
PECAM	Goat	polyclonal	1:100	Cy5	Santa Cruz	sc 1506
AKR1b7	Rabbit	polyclonal	1:750	AlexaFluor 488	Martinez A.	Ref.[2]
20 α-HSD	Rabbit	polyclonal	1:100	AlexaFluor 488	Weinstein Y.	Ref.[3]
3βHSD2	Rabbit	polyclonal	1:1000	AlexaFluor 488	Thomas M.	

1. Morohashi, K. et al. Functional difference between Ad4BP and ELP, and their distributions in steroidogenic tissues. Mol Endocrinol 8, 643-653 (1994).
2. Lefrancois-Martinez, A. M. et al. Decreased expression of cyclic adenosine monophosphate-regulated aldose reductase (AKR1B1) is associated with malignancy in human sporadic adrenocortical tumors. J Clin Endocrinol Metab 89, 3010-3019 (2004).
3. Piekorz, R.P., Gingras, S., Hoffmeyer, A., Ihle, J.N., and Weinstein, Y.. Regulation of progesterone levels during pregnancy and parturition by signal transducer and activator of transcription 5 and 20alpha-hydroxysteroid dehydrogenase. Mol Endocrinol 19, 431-440 (2005).

Figure S1 *Bandiera et al*

A

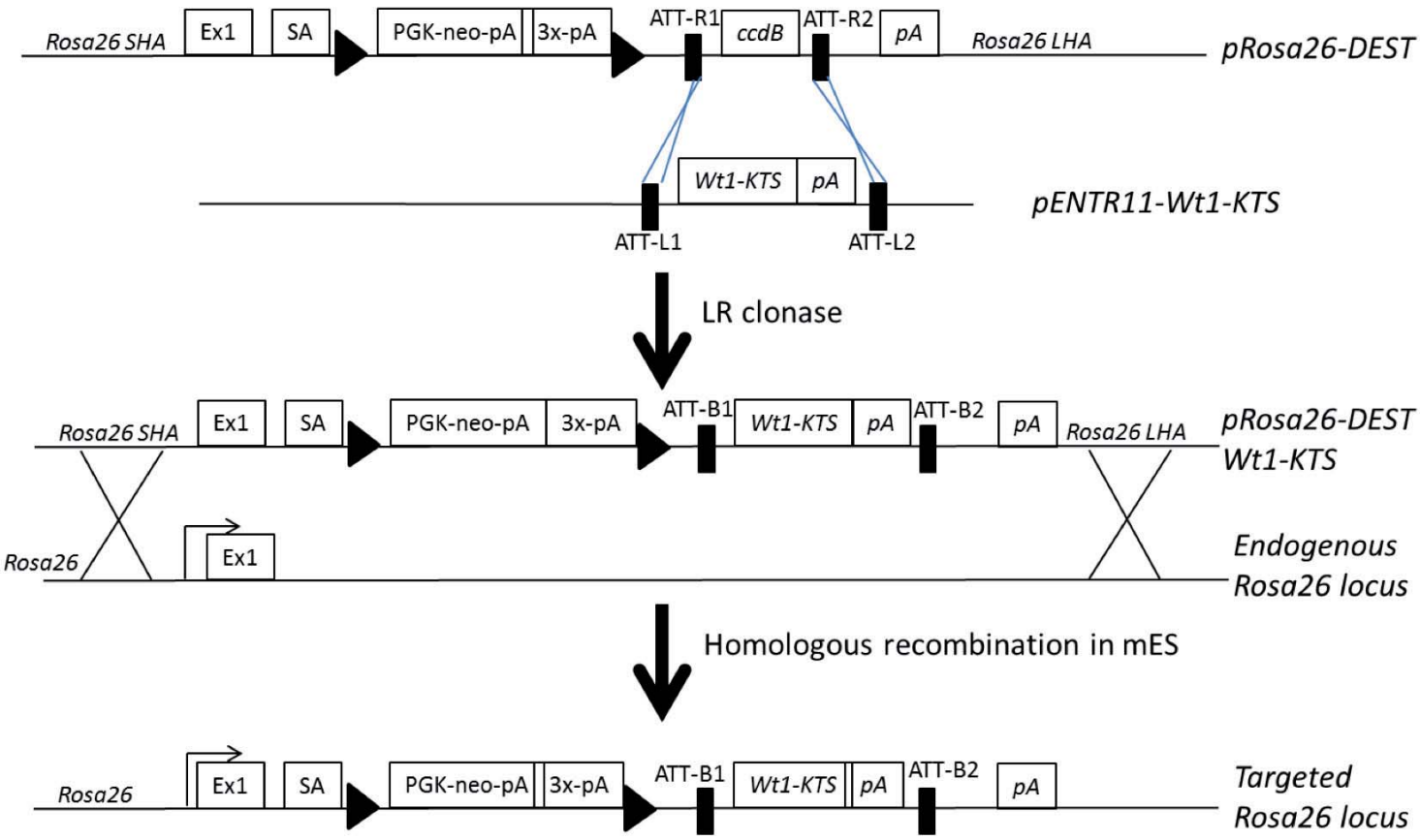

B

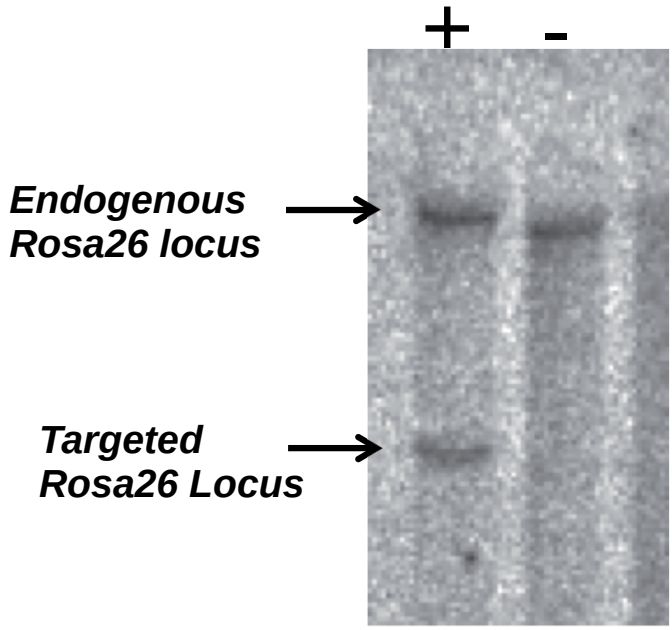

Figure S1 *Bandiera et al*

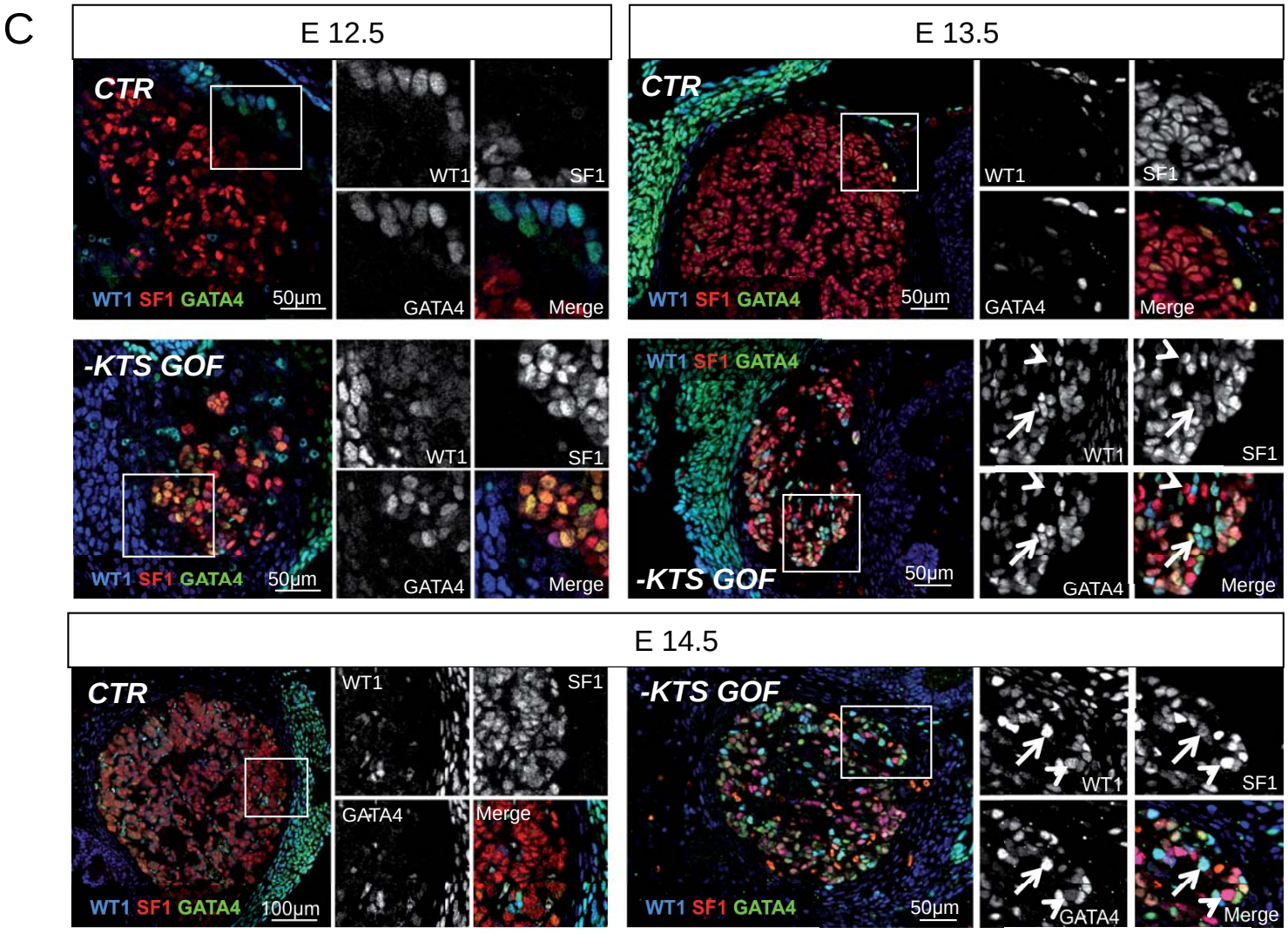

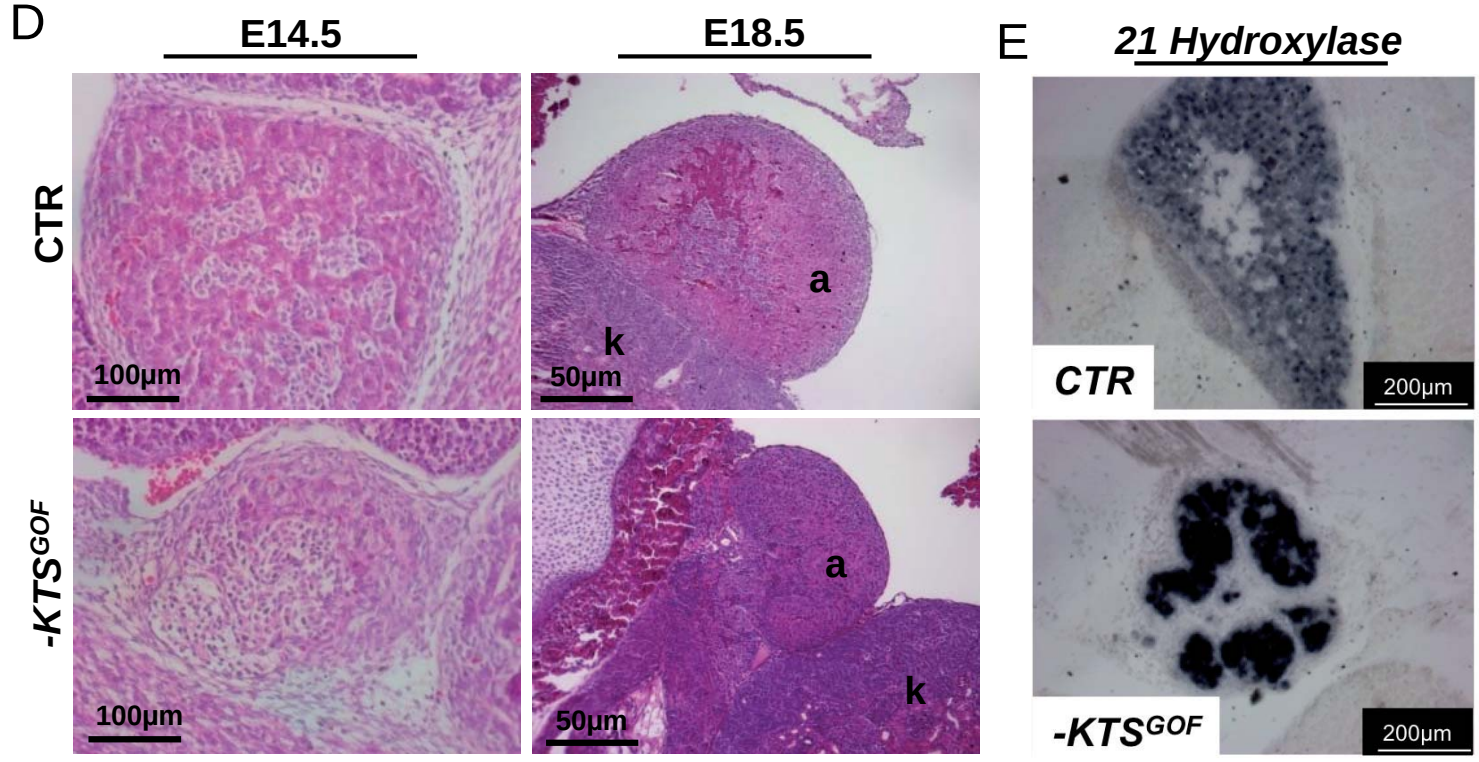

Figure S2 *Bandiera et al*

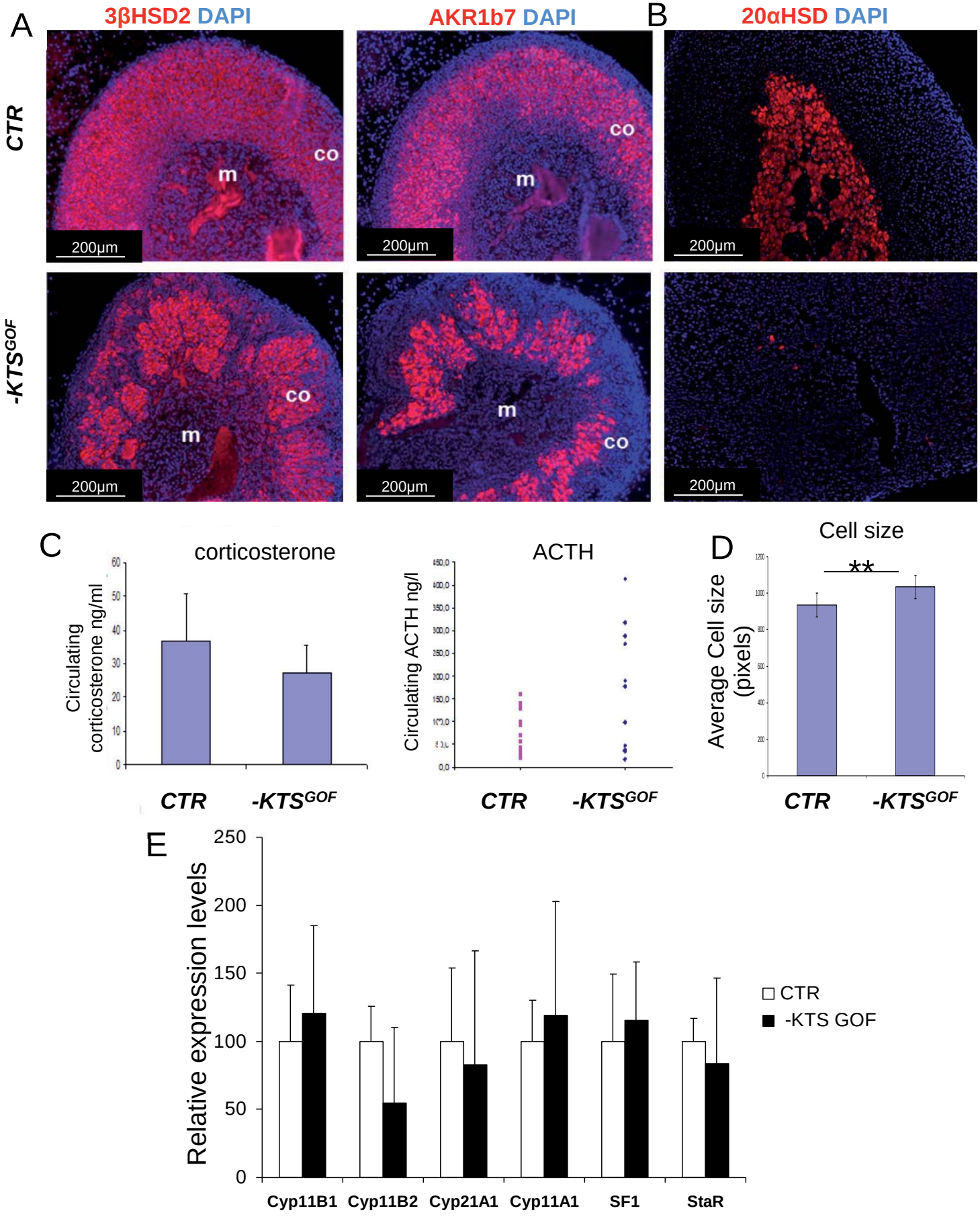

Figure S2 *Bandiera et al*

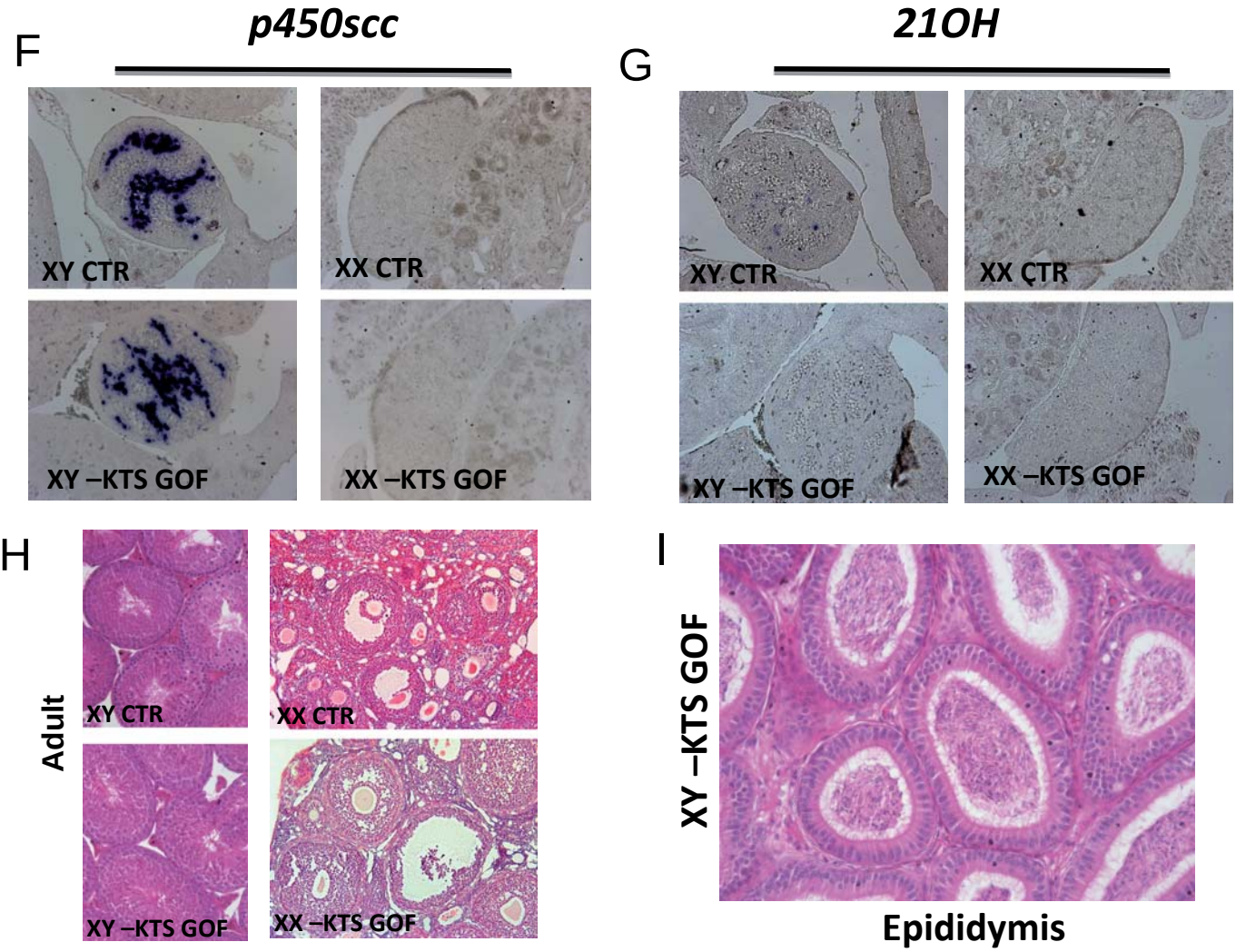

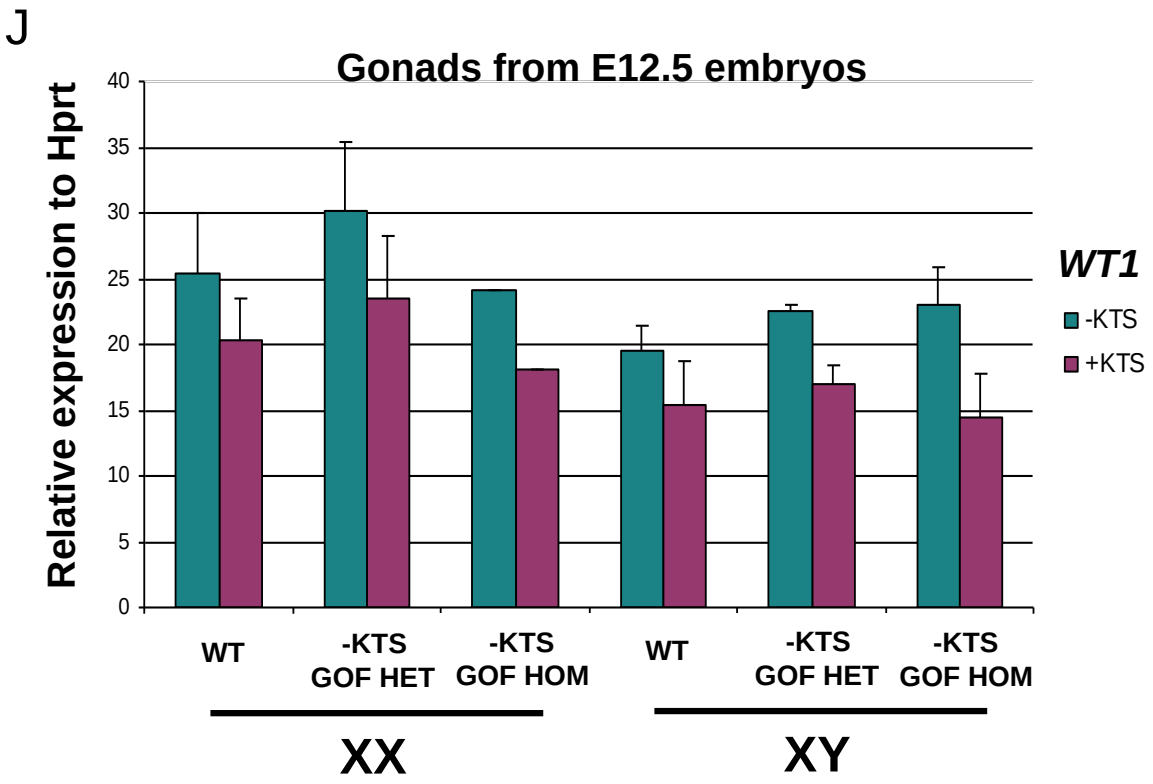

Figure S3 *Bandiera et al*

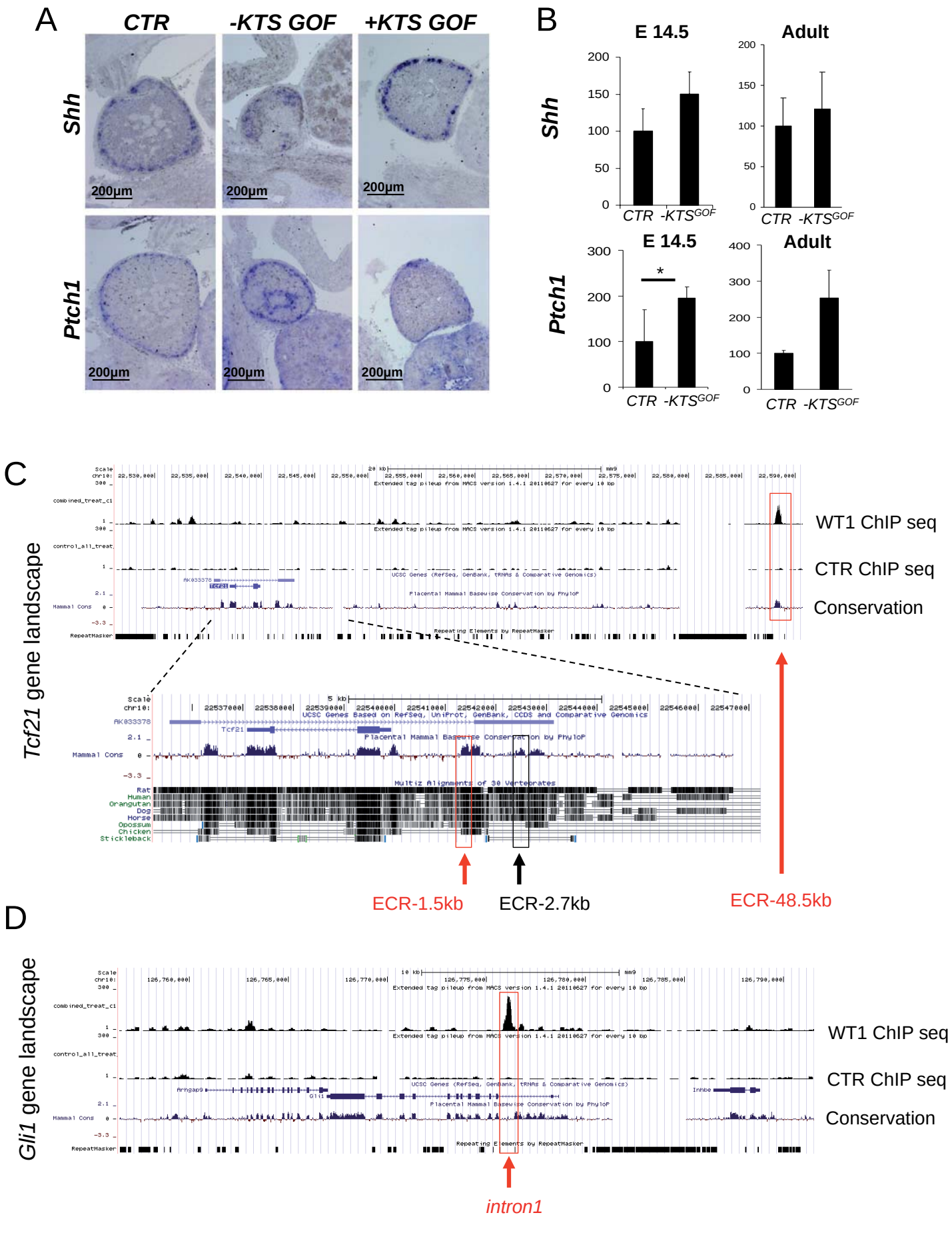

Figure S4

Bandiera et al

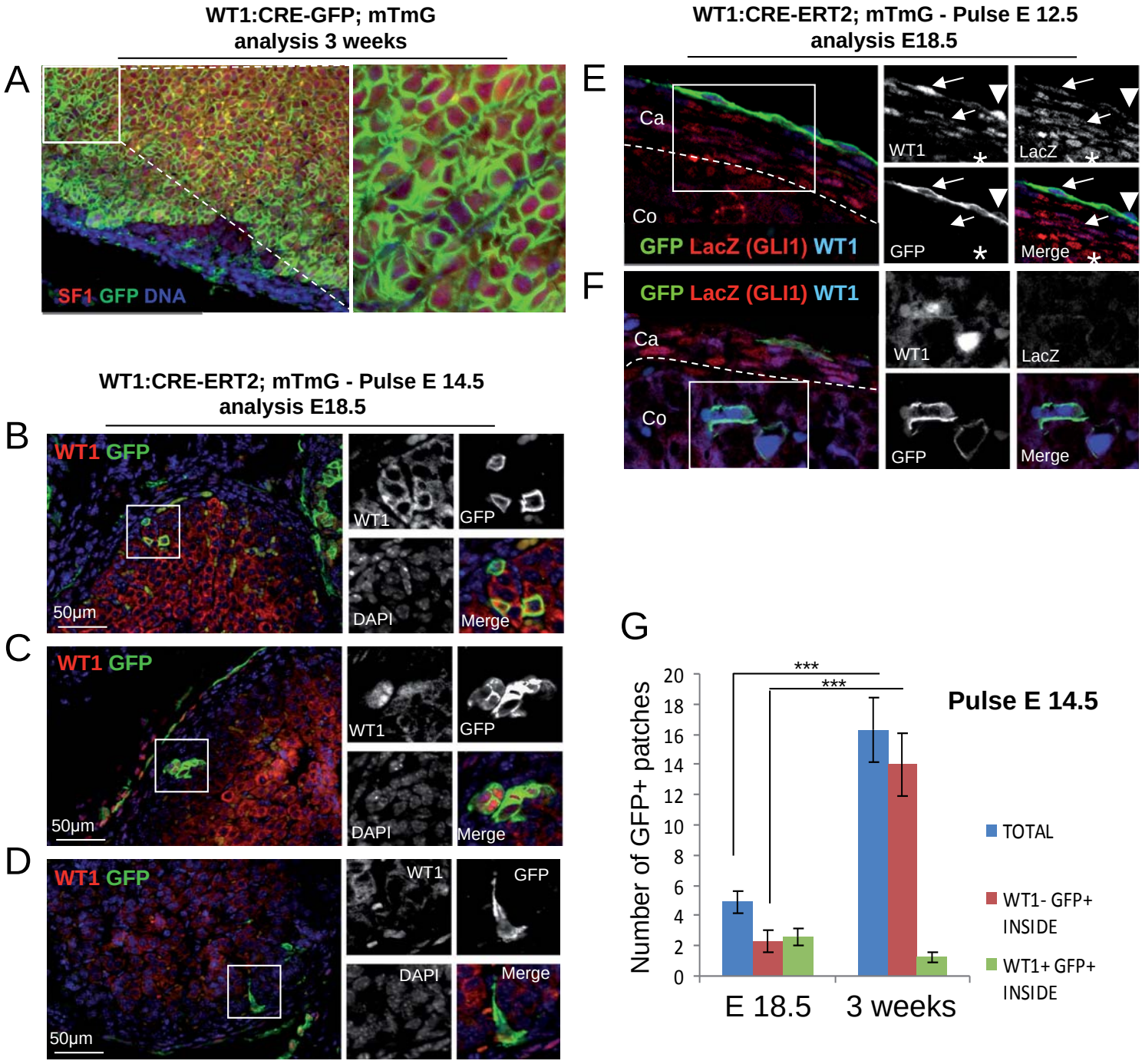

Figure S5 *Bandiera et al*

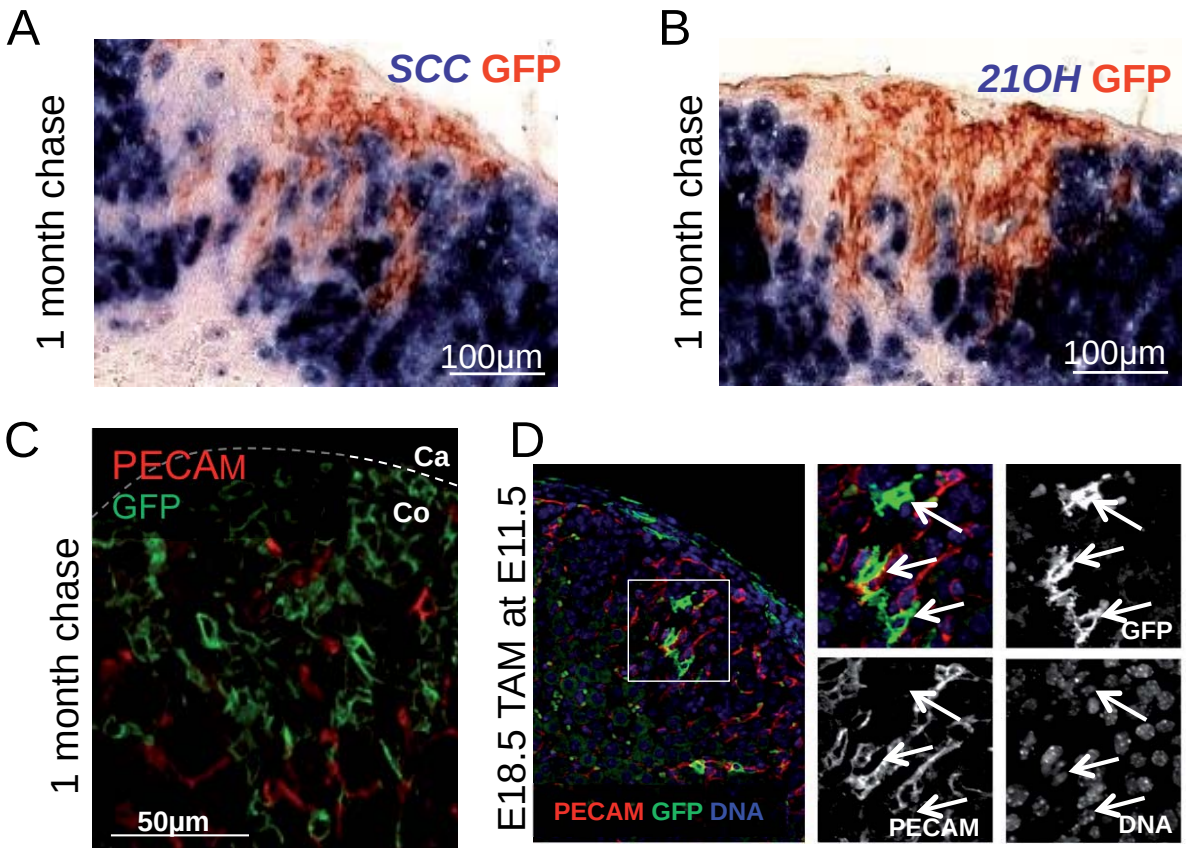

Figure S6 *Bandiera et al*

A

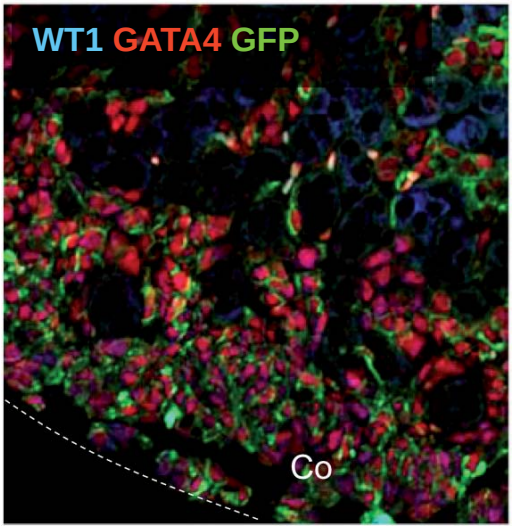

B

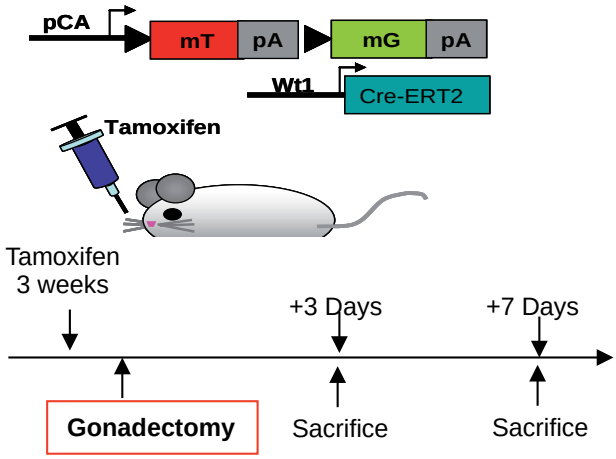

C

Males

Number of GFP+ patches within the cortex

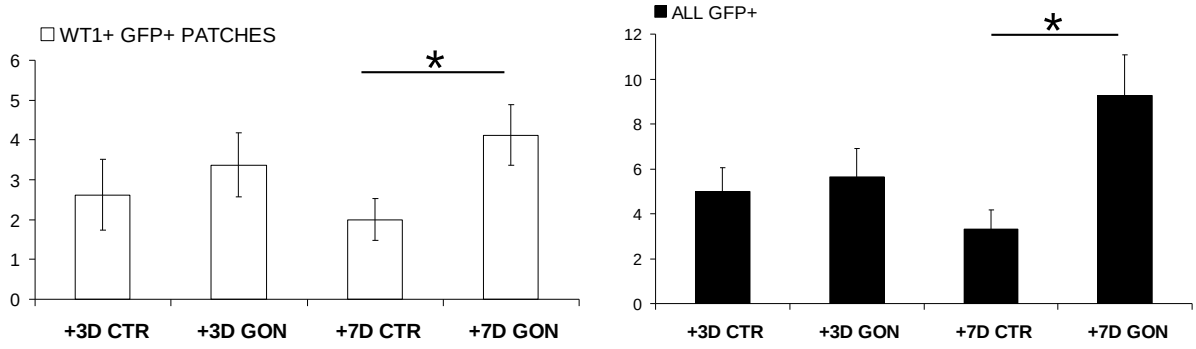

D

Females

Number of GFP+ patches within the cortex

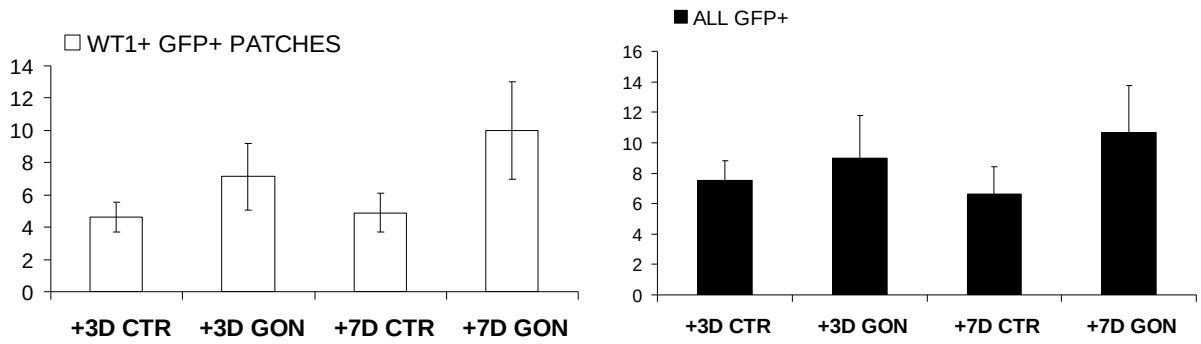

Table S1

	Weight
XX wild type	2.90 ±0.707 mg
XX -*KTS*^{GOF}	1.067 ± 0.404 mg
XY wild type	1.650 ± 0.20 mg
XY -*KTS*^{GOF}	0.760 ± 0.216 mg